Research Article

Evaluation of the 3D Topographic Effect of Homogeneous and Inhomogeneous Media on the Results of 2D Inversion of Electrical Resistivity Tomography Data

Marzhan Kabdykalievna Turarova [ID],[1] **Tolkyn Mirgalikyzy** [ID],[1]
Balgaisha Gafurovna Mukanova [ID],[2] **Igor Nikolaevich Modin** [ID],[3]
and Pavel Aleksandrovich Kaznacheev [ID][4]

[1]*Department of Computer and Software Engineering, L.N. Gumilyov Eurasian National University, Nur-Sultan 010008, Kazakhstan*
[2]*Astana IT University, Nur-Sultan 010000, Kazakhstan*
[3]*Department of Geophysical Methods of Earth Crust Study, M.V. Lomonosov Moscow State University, Moscow 119313, Russia*
[4]*The Schmidt Institute of Physics of the Earth of the Russian Academy of Sciences, Moscow 119313, Russia*

Correspondence should be addressed to Tolkyn Mirgalikyzy; m_t85@mail.ru

This work is devoted to the creation of numerical 3D models for studying 3D topographic effects of homogeneous and inhomogeneous media on the results of 2D inversion. To solve the direct problem, the integral equations method (IEM) was applied to simulate the electric field and calculate the values of apparent resistivity. For the numerical solution of the integral equation, a computational mesh, adapted to the terrain features, was constructed. The calculation of the apparent resistivity of the medium was implemented for a pole-dipole array. Calculations have been performed for a conducting medium with 3D local inhomogeneity and the ground surface topography. The influence of the 3D model with topography, flat ground surface, and immersed inhomogeneity on the results of 2D inversion was estimated. Influencing factors of the 3D model, such as the slope angle of the topography, the resistivity ratio of the inhomogeneity and the host medium, the average size of inhomogeneity and topography, the distance from the inhomogeneity to the measuring line for the medium with and without topography, and the distance between the electrodes of the electrical resistivity tomography (ERT) array, were studied. Based on the research results, recommendations and conclusions that can be useful when conducting geophysical studies by the ERT method are drawn.

1. Introduction

With the development of computer technologies and methods for solving direct and inverse problems, 2D and 3D electrical resistivity tomography (ERT) is widely used in geophysical research [1–6]. Among the main works that influenced the formation of ERT, we mention the Zohdy's work (the idea of a smooth 1D solution for electrical sounding). Barker transferred the ideas of a smooth solution from 1D problems to 2D [7, 8]. 2D ERT is a fast and efficient method of obtaining data on the geological structure for subsequent inversion and interpretation. 3D ERT is a new direc-

tion with a trend of future development; however, most measurements and interpretations are mainly based on 2D ERT [9–11]. Automatic 2D and 3D inversion programs are based on complicated algorithms for solving direct and inverse problems of electrical survey [12–24]. 2D and 3D inversions of ERT data often are carried out on the ground with an uneven surface; a high contrast of subsurface resistivity does not always give a real imaging of the geological structure [25–30]. The topography of the ground surface creates significant disturbances of the electric field, which in turn can generate strong anomalies in the results of inversion, which actually are not presented in real geological

structures [25–30]. This is because the array of electrical survey is located directly on the ground surface, where the contrast of resistivity between air and ground is usually much greater than the contrast between underground geological structures.

In 1935, Komarov and Gorbenko were the first to focus on the problem of the ground surface topographic effect on the electric field distribution [25, 26]. To date, the effects of the ground surface topography on the electric field and on the inversion results of ERT data remain one of the urgent problems of great scientific and practical interest.

In his thesis, Chanturishvili investigated the main features of the ground surface topographic effect on a homogeneous electric field for the case when a ridge or valley had the shape of an isosceles triangle [27]. He was convinced that the distortions of the vertical electrical sounding (VES) curves were not very noticeable for ridges and valleys with slope angles less than 20°, and that the distortions of the VES curves caused by ridges are greater than the distortions caused by valleys. It turned out that over the elevation angles of the topography, the values of apparent resistivity decrease, while over the descent angles of the topography, the VES curves increase. Yilmaz and Coskun noted that the inversion results of 2D ERT performed in areas with significant height changes may be erroneous, since the observed data on apparent resistivity may be distorted by topography [30].

The effect of the ground surface topography has been studied by many researchers, and several approaches have been developed to numerical account and reduction of this kind of effect at 2D and 3D data inversion [31–38].

Another potential problem in 2D surveys is the 3D effect, which produces anomalous artifacts when inverting ERT data. In 2D ERT, it is assumed that the resistivity of geological structures does not change in one of the horizontal directions, that is, the medium is considered as a 2D infinite half-space [39]. In reality, the geological structure is inhomogeneous in three directions, and electric current flows in 3D space (X, Y, and Z), and therefore, the results of 2D ERT may be erroneous [40, 41]. The 3D effect means that the geological 3D structure outside the resistivity profile will affect the results of 2D inversion in the form of artifacts [39]. Also, using a 2D inverse program, assuming that the topography is 2D, will give incorrect results since the topography is 3D.

Dahlin, Lin et al., and Bievre et al., in their studies, noted the influence of the 3D effect on the results of 2D ERT and suggested to take into account 3D effects in interpretation and inversion [42–44]. Hojat et al. also noticed the influence of the 3D geometry of a particular object on the 2D ERT data that were measured using the monitoring system of the internal hydrogeological state of the dam [45]. According to the results of their study, regardless of the lateral position of the profiles, all measurements along the embankment are distorted by 3D effects, especially in the deeper parts. In [39], Tresoldi et al. have applied the developed strategy to correct such effects in the initial data obtained along river dams. They have observed that their method reasonably eliminates such effects, but this problem remains an urgent area of research that should be developed for conducting accurate correction.

The purpose of the present work is to study the 3D topographic effect with a homogeneous and inhomogeneous structure of the ground on the results of 2D ERT inversion. In this work, 3D conducting media with 3D local inhomogeneity and the ground surface topography are simulated by creating a numerical model for calculating apparent resistivity employing the integral equations method (IEM). To study the 3D topographic effect on the results of 2D ERT data inversion, we make parametric changes in the slope angle of the topography, the resistivity ratio of the inhomogeneity and the host medium, the average size of inhomogeneity and topography, the distance from the inhomogeneity to the measuring line for the medium with and without topography, and the distance between the electrodes of the ERT array. Based on the results of numerical simulation, recommendations and precautions have been made for future tests and fieldwork while interpreting 2D ERT data with a real 3D topography.

2. Simulation of Apparent Resistivity Using IEM

To simulate the apparent resistivity curves of the studied media, the IEM was applied [46], which can also be interpreted as an implementation of the boundary element method (BEM).

Using IEM for simulation, the electric field has well recommended itself [47–51] and has advantages in cost-effectiveness of computing resources compared to finite element method (FEM) and finite difference method (FDM). In the IEM, the computational mesh is built on the contact boundaries of the media only, whereas in finite element and finite difference methods, the mesh is built on a 3D computational volume [52, 53].

To simulate the electric field, in the presented study, a computational mesh is built only on the surfaces of the ground and the immersed inhomogeneity (see Figure 1). The mesh is adapted to the measuring line. The measuring line is located along the x-axis.

The mesh on the ground surface is refined along the measuring line (see Figure 2).

In the developed program, data collection is simulated using a pole-dipole array ($AMN + MNB$), which widely used in ERT studies. In the case of measuring by a pole-dipole array AMN, the second source B is referred to the physical infinity, and for pole-dipole array MNB, source A is referred to infinity. For a pole-dipole array AMN, the apparent resistivity of the medium is calculated using the following formula:

$$\rho_k = K \frac{\Delta U_{MN}}{I_A}, K = \frac{2\pi \cdot AM \cdot AN}{MN}. \tag{1}$$

where K is the geometric coefficient for this array (AMN), ΔU_{MN} is the measured potential difference between the receiving electrodes M and N, A is the supply electrode, and I_A is the current in the supply line.

The structure of the output files was adapted to the format of 2D inversion programs.
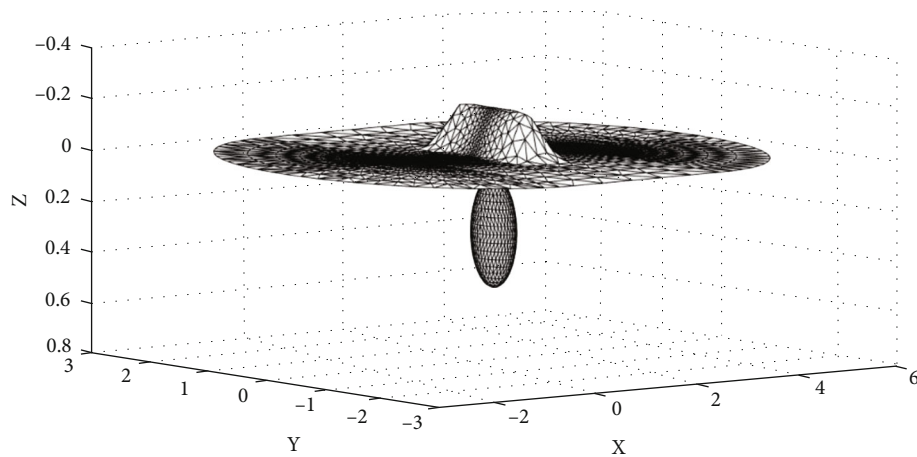
FIGURE 1: 3D model of the computational mesh for simulating the electric field by IEM for the medium with the ground surface topography and immersed inhomogeneity.

A-Supply electrode;
M, N-measuring electrodes;
Len_{sur}-Measuring line;
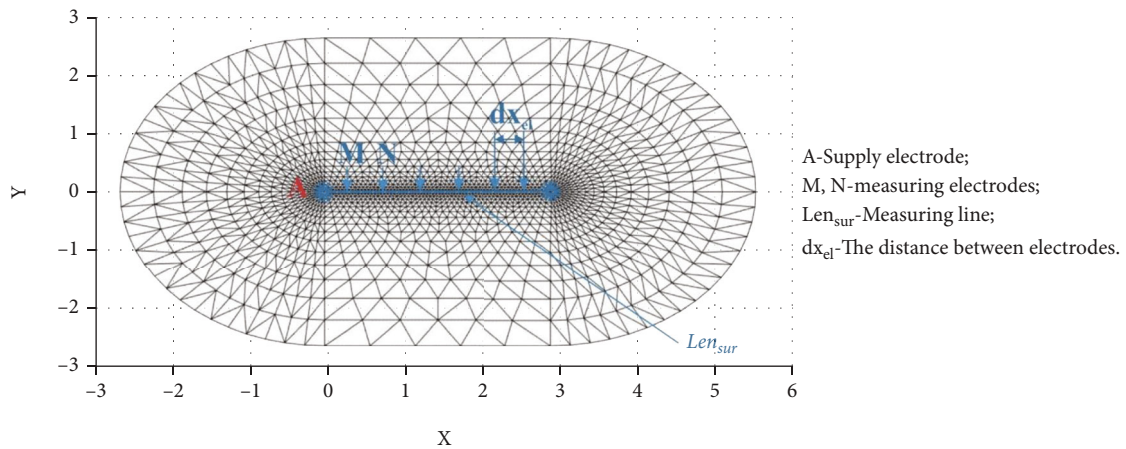dx_{el}-The distance between electrodes.

FIGURE 2: Computational mesh for simulating the electric field by IEM on the ground surface (top view on XY plane).

The numerical implementation of the algorithm for calculating the apparent resistivity curves of the IEM for a topography with 3D immersed inhomogeneity is compared with the results obtained by the FEM. To compare two methods, the authors used the COMSOL Multiphysics software, where the direct problem of ERT is solved by FEM [54, 55].

3D computational mesh for the FEM used for modeling in the COMSOL Multiphysics sofware is represented in Figure 3. To simulate the electric field by FEM, the total computational volume has been defined before. The simulated volume is chosen in such a way that its limitation in space does not affect the solution in the area of interest. For testing purpose, the simulated volume was set as a hemisphere. The radius of the sphere is 1000 m. Figure 3 shows only a quarter of the sphere. Figure 4 shows only a part of the simulated volume containing the area of interest (topography element and heterogeneity). The supply electrode is installed in the center of the hemisphere.

The simulated volume is divided into finite elements of tetrahedra. The mesh thickens near the current source, the
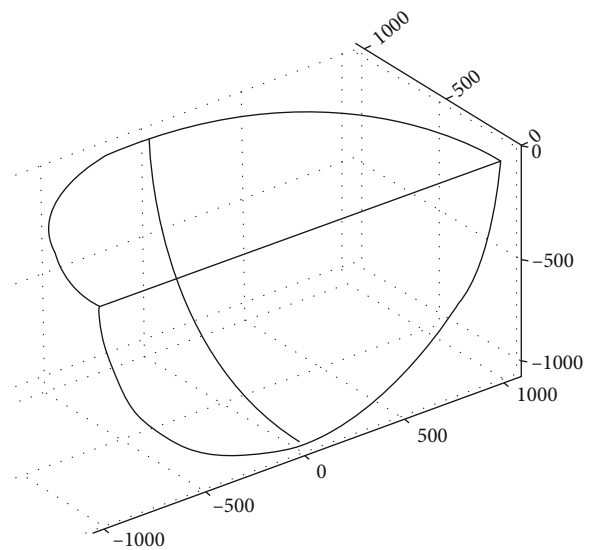

FIGURE 3: Simulated volume constructed in the COMSOL Multiphysics program (FEM).
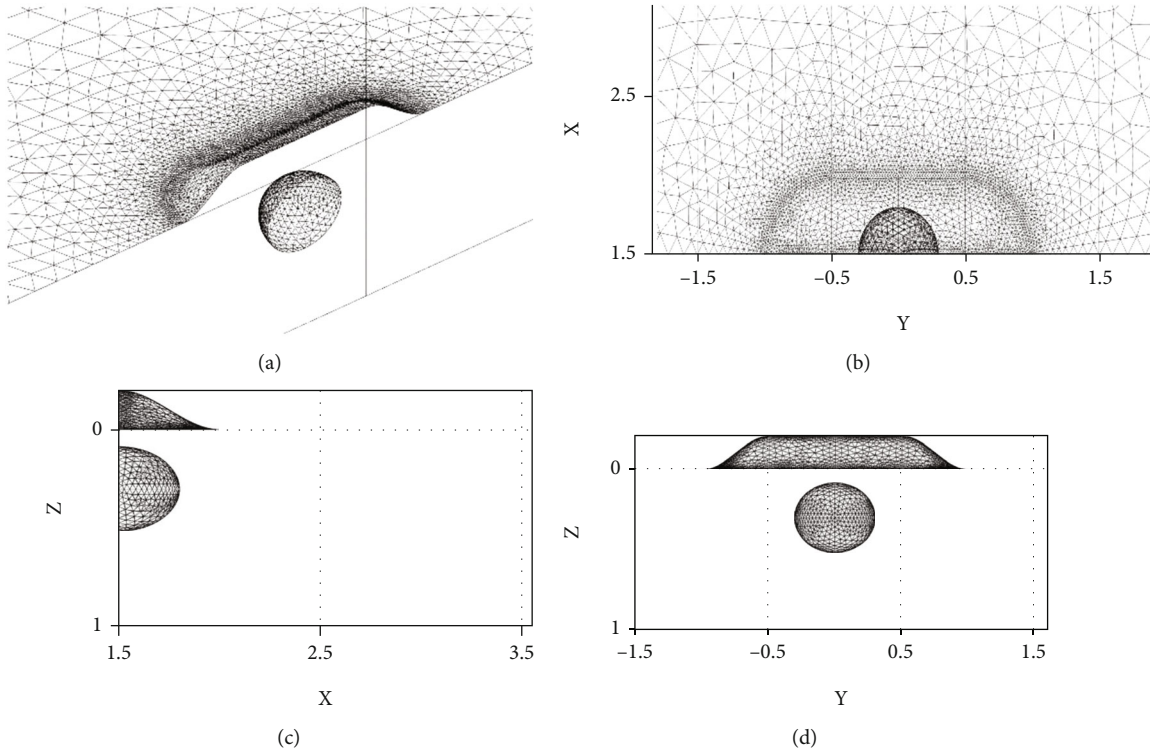
(a)

(b)

(c)

(d)

FIGURE 4: The mesh of the studied area of the simulated volume in the COMSOL Multiphysics program (FEM): (a) orthographic projection view, (b) plan view, and (c and d) cross-sectional views. For convenience, only half of the model on the x-axis is shown.

(a)

(b)

(c)

dx_{ter}-The length of the topography base along the X-axis;
dy_{ter}-The width of the topography base along the Y-axis;
dx_{het}-The size of the inhomogeneity diameter along the X-axis;
dy_{het}-The size of the inhomogeneity diameter along the Y-axis;
dz_{het}-The size of the inhomogeneity diameter along the Z-axis;
$depz_{het}$-The depth of the upper part of the inhomogeneity;
$disy_{bet}$-The distance between the inhomogeneity and the measuring line along the Y-axis;
α-The slope angle of the topography;
ρ_1-The resistivity of the medium;
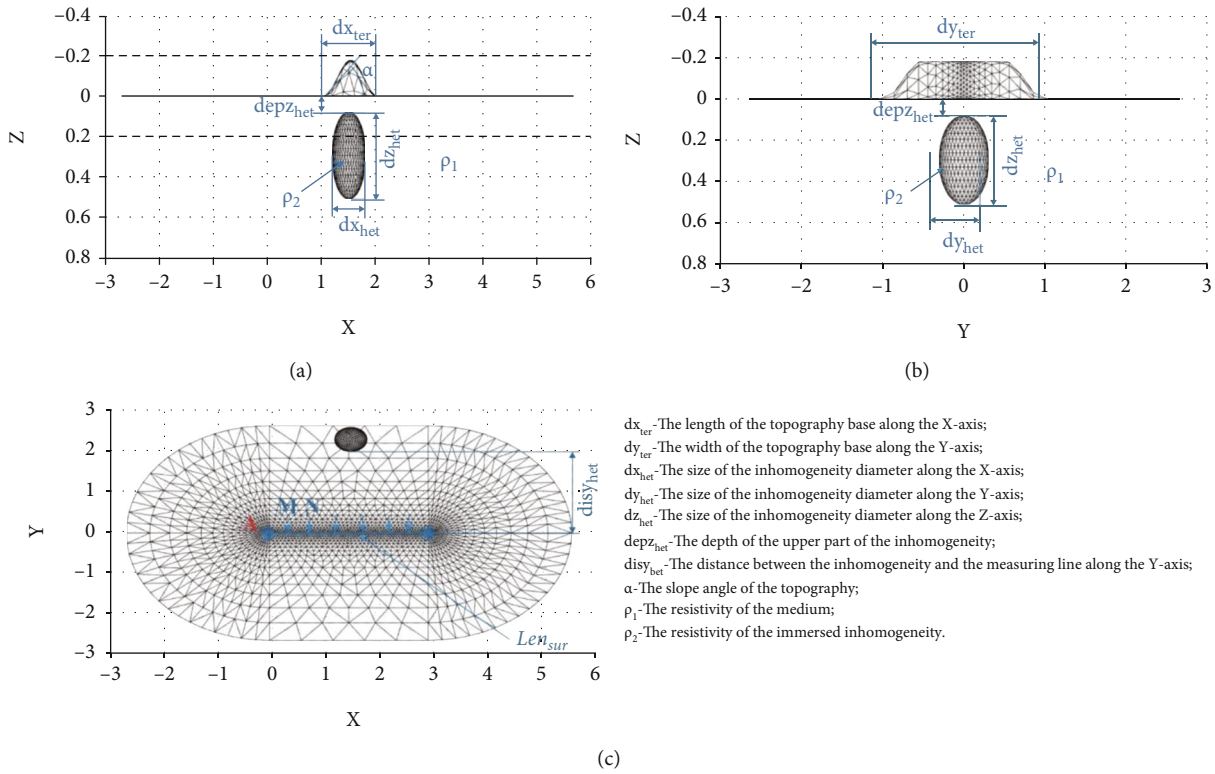ρ_2-The resistivity of the immersed inhomogeneity.

FIGURE 5: Computational mesh on the ground surface and immersed inhomogeneity surface. (a) XZ-section. (b) YZ-section. (c) Computational mesh on the ground surface in the XY-section (Bottom view).

TABLE 1: Explanatory table of 3D model influence parameters.

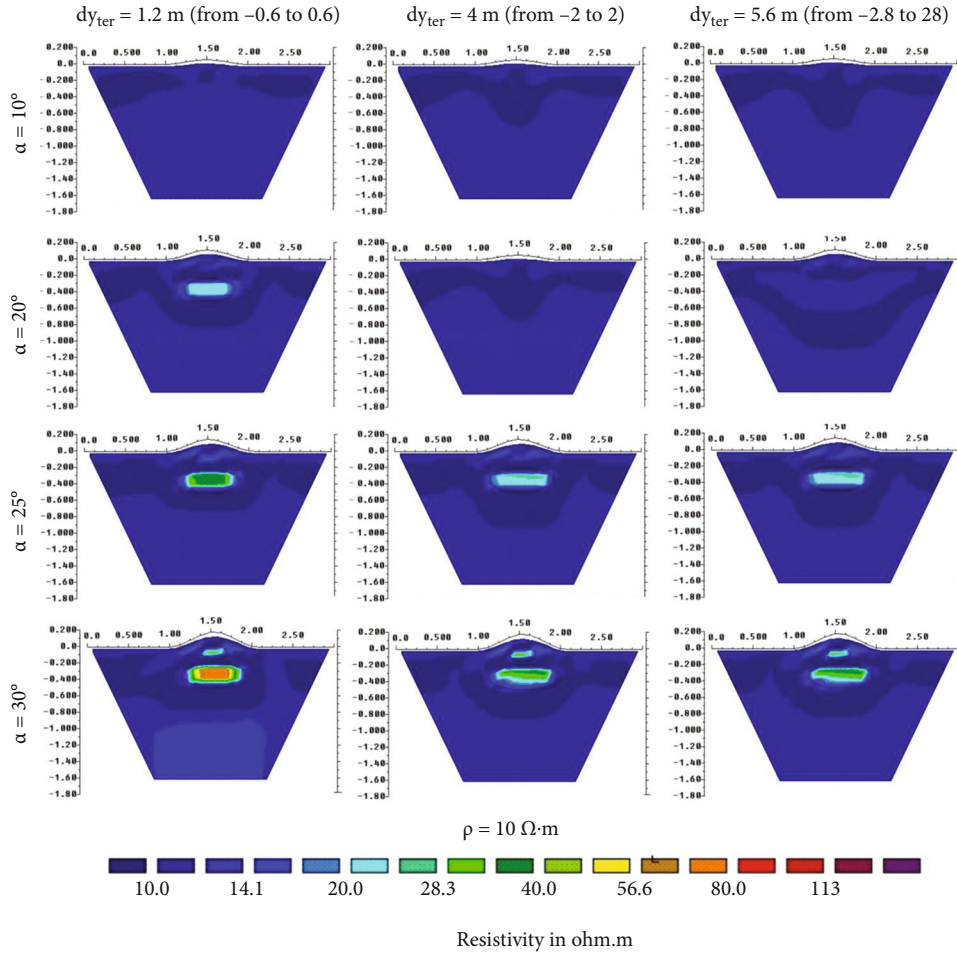| Influence factor (of 3D effect)	ρ_1 $(\Omega \cdot m)$	ρ_2 $(\Omega \cdot m)$	α, °	$dx_{ter(m)}$	$dy_{ter(m)}$	$dx_{het(m)}$	$dy_{het(m)}$	$dz_{het(m)}$	$xc_{het(m)}$	$yc_{het(m)}$	$zc_{het(m)}$	$disy_{het(m)}$	Num_{el}	$dx_{el(m)}$
The slope angle of the topography and the length of the topography along the y-axis(homogeneous medium)	6	10	10° 20° 25° 30°	1	1.2 4 5.6	—	—	—	—	—	—	—	24	0.125
Resistivity contrast ratio ($n = \rho_2/\rho_1$) ($\rho_1 < \rho_2$)	10	20 40 60 80 100	30°	1	1.2 5.6	0.6	0.6 5.6	0.43	1.5	0	0.3	—	24	0.125
Resistivity contrast ratio ($n = \rho_2/\rho_1$) ($\rho_1 > \rho_2$)	20 40 60 80 100	10	30°	1	1.2 5.6	0.6	0.6 5.6	0.43	1.5	0	0.3	—	24	0.125
The size of the inhomogeneity in the Y-direction (medium without topography)	10 40	40 10	0°	—	—	0.6	0.6 1.2 2 4 5.6	0.43	1.5	0	0.3	—	24	0.125
The size of the inhomogeneity and topography in the Y-direction (medium with topography)	10 40	40 10	30°	1	0.6 1.2 2 4 5.6	0.6	0.6 1.2 2 4 5.6	0.43	1.5	0	0.3	—	24	0.125
Inhomogeneity distance from the measuring line (medium without topography)	10 40	40 10	0°	—	—	0.6	0.6	0.43	1.5	0.3 0.6 1.3 1.8 2.3	0.3	0 0.3 1 1.5 2	24	0.125
Inhomogeneity distance from the measuring line (medium with topography)	10 40	40 10	30°	1	0.6 1.2 2 4 5.6	0.6	0.6	0.43	1.5	0.3 0.6 1.3 1.8 2.3	0.3	0 0.3 1 1.5 2	24	0.125
Distance between measuring electrodes	10	10	30°	1	1.2	—	—	—	—	—	—	—	24 48	0.125 0.0625

FIGURE 6: The influence of the topography slope angle along the x-axis and the topography width of the 3D homogeneous medium in the Y-direction on the results of 2D inversion.

angles of the inhomogeneity bends, and the ground surface relief. The computational mesh turns out to be very cumbersome, taking into account the partitioning of the entire volume surface and not just the distribution surface of the electric current. The geometry of the model is located closer to the center of the total simulated volume, that is, closer to the supply electrode. Figure 4 shows the computational mesh (FEM) of a 3D model for the ground surface relief and inhomogeneity in the shape of an ellipsoid. Due to the large simulated volume, a lot of grid elements are located in the remaining part of the simulated volume. To reduce their number, it is necessary to use an uneven grid or special boundary conditions.

20,104 triangulation elements were used to simulate the electric field by IEM. Accordingly, about 200,000 three-dimensional finite elements were used for the FEM.

Testing was carried out for various 3D models of the media: for uneven and smooth ground surfaces with immersed 3D inhomogeneity and without inhomogeneity.

According to the test results, to obtain smoother results, the FEM required almost 10 times more number of elements of the computational mesh and much more time. This shows that the developed numerical algorithm for simulating

apparent resistivity curves using IEM has advantages in performance and economy. IEM calculations require significantly less computing resources.

3. Numerical Models

To understand the influence of the 3D topographic effect of a homogeneous and inhomogeneous medium, various numerical models were created in this study (see Figure 5). Then, we investigated the possible influence of the 3D topographic effect on the results of 2D ERT inversion using changes of parameters, such as the slope angle of the topography, the resistivity ratio of the inhomogeneity and the host medium, the average size of inhomogeneity and topography, the distance from the inhomogeneity to the measuring line for the medium with and without topography, and the distance between the electrodes of the ERT array.

In this study, ρ_1 is the resistivity of the medium, and ρ_2 is the resistivity of the immersed inhomogeneity. The ratio of ρ_1 and ρ_2 was denoted as the resistivity contrast ratio $n = \rho_2/\rho_1$.

The topography of the ground surface has the shape of a 3D hill, the slope angle of the topography along the x-axis is
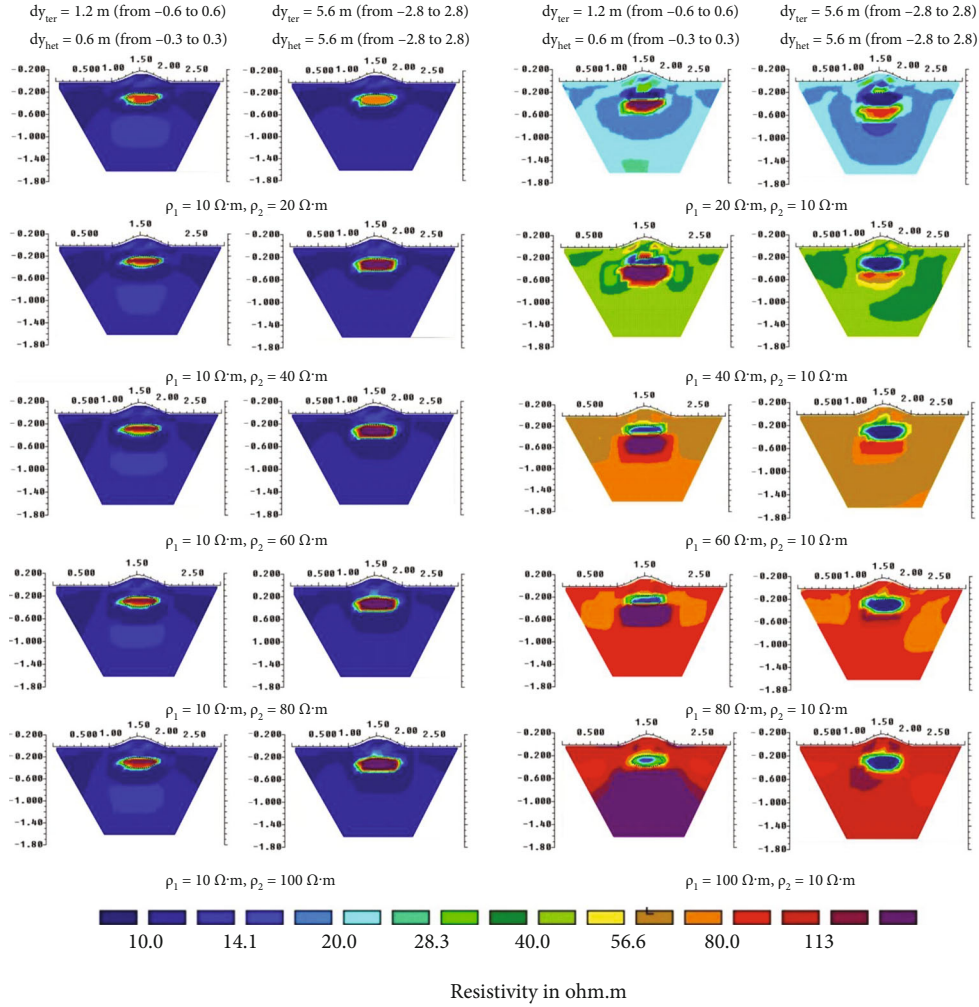
FIGURE 7: The influence of the resistivity contrast ratio of a 3D inhomogeneous medium with the ground surface topography on the results of 2D inversion.

designated as α, the length of the topography base along the x-axis is dx_{ter}, and the width of the topography base along the y-axis is dy_{ter}. In the calculations, a certain value L was set as a unit of length, and further, all the geometric dimensions of the models and the measuring setup were expressed in these units. In the models discussed here, the length of the measuring line $Len_{sur} = 3$ (Figure 2), i.e., the unit of length L is one-third of Len_{sur}. To switch to dimensional values, it is necessary to multiply all dimensionless geometric parameters by the value L in meters. The length of the topography dx_{ter}, expressed in units of L, was assumed to be constant, and the length of the sounding line Len_{sur} in meters is $3\,L$.

Let us denote topography base centers along the x- and y-axes as xc_{ter} and yc_{ter}; xc_{ter} corresponds to 1.5, and yc_{ter} corresponds to the coordinate center 0.

The immersed inhomogeneity has the shape of an ellipsoid, that dimensions along the X, Y, Z are equal to dx_{het}, dy_{het}, and dz_{het}, respectively. The coordinates of the immersion depth of the heterogeneity center are denoted by xc_{het}, yc_{het}, and zc_{het}, and the $depz_{het}$ is the depth of the upper part of the inhomogeneity. In all calculation models, a small

inhomogeneity immersion depth is chosen, where it is well detected. Therefore, to study the 3D effect of immersed inhomogeneity, in the present study, the immersion depth of the center and the depth of the upper part of the inhomogeneity remain constant $zc_{het} = 0.3$ m, $depz_{het} = 0.085$ m ≈ 0.1 m. xc_{het} is also fixed to 1.5; $disy_{het}$ is the distance of the inhomogeneity location from the measuring line along the y-axis.

The distance between the measuring electrodes is denoted as dx_{el}, and their number – Num_{el}. The profile line is directed along the x-axis.

Artifacts are caused by a change in the topography in the YZ plane because 2D inversion programs assume that the topography continues from minus to plus infinity in the Y-direction.

Due to the truncation of the topography in the Y-direction, the program interprets the air behind the hill in the Y-direction as an increase in resistivity [39]. Therefore, in our study, we evaluated the width of the hill and the heterogeneity in the Y-direction relative to the length of the survey line as an important factor causing artifacts. We changed the

parameters of the topography width dy_{ter} and inhomogeneity dy_{het} in the Y-direction relative to the survey line. The slope angle α of topography in the X-direction was also changed, since with the change in the slope of the topography, the height and volume change, respectively, which also affect the appearance of artifacts resulting from 2D inversion. Explanatory Table 1 presents the values of the model parameters for studying and evaluating the appearance of artifacts using 2D inversion of ERT data. To study the 3D effect in the results of 2D inversion, the Res2Dinv (3.55 version) program was used.

4. Results and Discussion

4.1. Influence Factors of the 3D Model

4.1.1. Influence of the Slope Angle and the Width of the Topography along the y-Axis. As noted above, an important factor distorting the results of 2D ERT inversion is the width of the topography in the Y-direction compared to the length of the survey line. Here, a model of a homogeneous medium with the ground surface topography was considered. The resistivity of a homogeneous medium was set as $\rho = 10\,\Omega \cdot m$. To enter the calculation results into the Res2Dinv program, it is necessary to specify the length scale L. The numerical values of the geometric parameters shown in Table 1 correspond to $L = 1\,m$.

Comment. In this study, a relatively small scale $L = 1\,m$ was used for simulation purposes. However, the results obtained remain valid for arbitrary L at a corresponding proportional change in geometric dimensions.

In the present study, at different slope angles along the x-axis ($\alpha = 10°$, $20°$, $25°$, and $30°$), three different sizes of topography width were established: dy_{ter} =1.2 m (from -0.6 to 0.6), 4 m (from -2 to 2), and 5.6 m (from -2.8 to 2.8) along the y-axis. The influence of the topography slope angle and the topography width of the 3D homogeneous medium in the Y-direction on the results of 2D inversion are shown in Figure 6.

When the topography slope angle along the x-axis is equal to $\alpha = 10°$, and minor artifacts from the ground surface topography are noticeable, which can be neglected. When the topography slope angle along the x-axis is $\alpha = 20°$, one can notice the influence of the 3D topography effect. At a topography width $dy_{ter} = 1.2\,m$ (from -0.6 to 0.6), 3D effect is noticeable, and at a topography width $dy_{ter} = 4\,m$ (from -2 to 2) and $dy_{ter} = 5.6\,m$ (from -2.8 to 2.8), no noticeable 3D effect was detected. Starting from the topography slope angle $\alpha = 25°$, one can notice the presence of a 3D topographic effect in all cases. However, at the topography width $dy_{ter} = 1.2\,m$, with an increase in the topography slope angle ($\alpha = 30°$), the dependence of resistivity of the anomalous zone on the 3D topographic effect becomes stronger.

At a topography width $dy_{ter} = 1.2\,m$, the edge of the hill at a distance of 0.6 m from the survey line is only 1/5 of the length of a 3-meter survey line, and this, as we see, leads to serious artifacts.

At a topography width $dy_{ter} = 4\,m$, the edge of the hill at a distance of 2 m from the survey line is about 3/2 of the length of the 3-meter survey line, and at a topography width

dy$_{het}$ = 0.6 m (from –0.3 to 0.3)

dy$_{het}$ = 1.2 m (from –0.6 to 0.6)

dy$_{het}$ = 2 m (from –1 to 1)

dy$_{het}$ = 4 m (from –2 to 2)

dy$_{het}$ = 5.6 m (from –2.8 to 2.8)

$\rho_1 = 10\,\Omega \cdot m,\ \rho_2 = 40\,\Omega \cdot m$ $\rho_1 = 40\,\Omega \cdot m,\ \rho_2 = 10\,\Omega \cdot m$

10.0   14.1   20.0   28.3   40.0   56.6   80.0   113
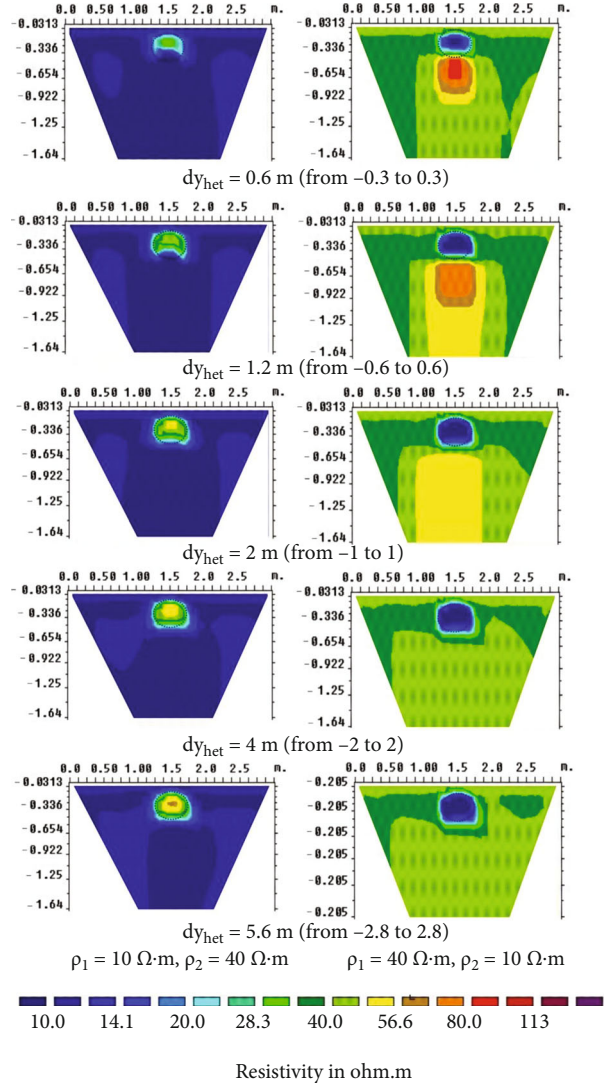
Resistivity in ohm.m

FIGURE 8: The influence of the inhomogeneity's size of a 3D medium with a flat ground surface in the Y-direction on the results of 2D inversion.

$dy_{ter} = 5.6\,m$, the edge of the hill at a distance of 2.8 m is almost comparable to the length of the survey line, and in this case, artifacts weaken.

4.1.2. Resistivity Contrast Ratio. To understand the influence of the resistivity contrast ratio of an inhomogeneous medium with the ground surface topography on the 3D effect in the results of 2D ERT data inversion, ten different values of the resistivity contrast ratio ($n = \rho_2/\rho_1$) were considered: five of them corresponded to $\rho_1 < \rho_2$ ($n = 2, 4, 6, 8,$ and 10) and another five – to $\rho_1 > \rho_2$ ($n = 0.5, 0.25, 0.17, 0.125,$ and 0.1). To discuss the influence of the resistivity contrast ratio, we set ρ_1 as $10\,\Omega \cdot m$ when $\rho_1 < \rho_2$ and set ρ_2 as 20, 40, 60, 80, and 100 $\Omega \cdot m$, respectively. For the case when $\rho_1 > \rho_2$, ρ_2 was set to $10\,\Omega \cdot m$, and ρ_1 to 20, 40, 60, 80, and 100 $\Omega \cdot m$, respectively.

For testing, models of an uneven ground surface with a topography slope angle $\alpha = 30°$ and two topography widths
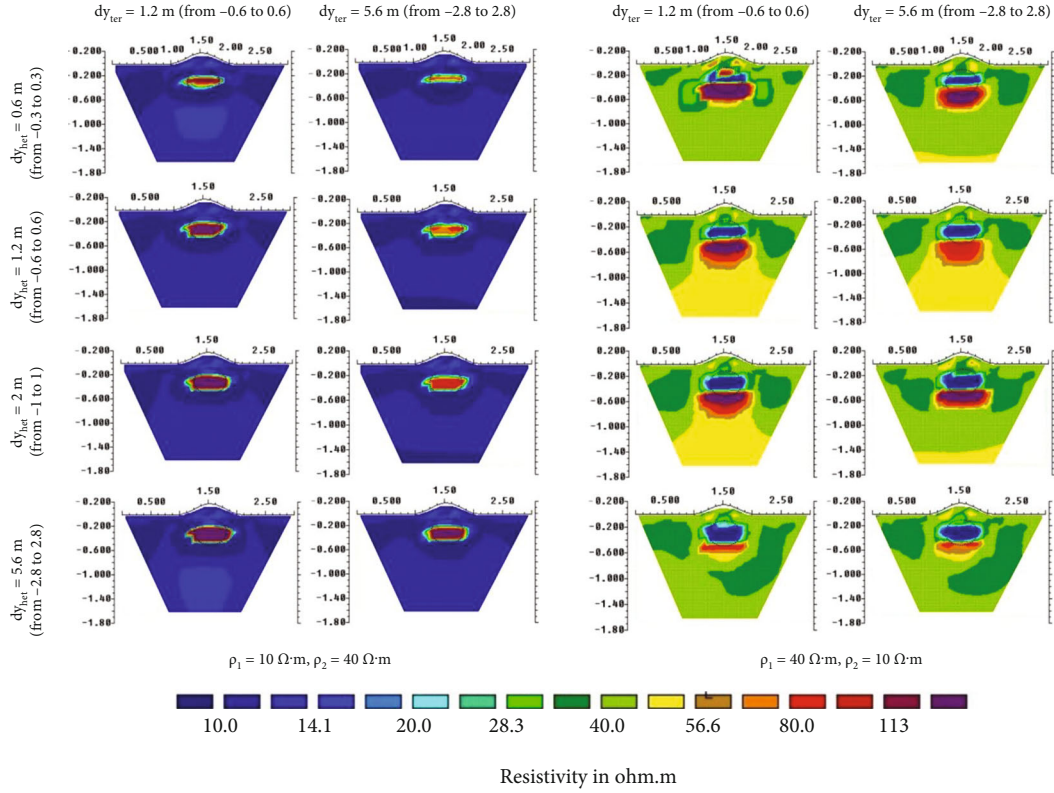
FIGURE 9: The influence of the inhomogeneity's size of a 3D medium with the ground surface topography in the Y-direction on the results of 2D inversion.

equal to $dy_{ter} = 1.2$ m (from -0.6 to 0.6) and 5.6 m (from -2.8 to 2.8) along the y-axis were selected, where the contrast of the 3D topographic effect is well noticed. Two sizes of inhomogeneity under the ground surface topography in the Y-direction are given, namely, $dy_{het} = 0.6$ m with a small edge distance (from -0.3 to 0.3) and $dy_{het} = 5.6$ m with a large edge distance (from -2.8 to 2.8) perpendicular to the survey line. yc_{ter} is at the origin of the coordinates.

The influence of the resistivity contrast ratio of a 3D inhomogeneous medium with the ground surface topography on a 2D inversion is shown in Figure 7.

Consider the case $\rho_1 < \rho_2$. When the resistivity contrast ratio is $n = 2$, at a small contrast, the predominance of 3D topographic effect can be observed at given topography widths $dy_{ter} = 1.2$ m (from -0.6 to 0.6) and 5.6 m (from -2.8 to 2.8). Starting with the resistivity contrast ratio $n = 4$, one can notice the mixing and strengthening of the resistivity of the anomalous zone in the geological section of 2D inversion.

When the edges of the inhomogeneity and the ground surface topography are at a short distance from the measuring line in the Y-direction ($dy_{ter} = 1.2$ m (from -0.6 to 0.6) and $dy_{het} = 0.6$ m (from -3 to 3)), the 3D topographic effect affects more strongly, and the shape of the anomalous zone is essentially flattened out in the horizontal direction and the resistivity increases.

When the distances of the edges of the inhomogeneity and the ground surface topography increase in the Y-direction ($dy_{ter} = 5.6$ m (from -2.8 to 2.8) and $dy_{het} = 5.6$ m

(from -2.8 to 2.8)) relative to the length of the measuring line, a more circular shape of the anomalous zone under the topography is observed. It is noticeable that the effect of identifying the shape of inhomogeneity under the topography becomes clearer. However, the resistivity is also amplified and mixed, that is, the 3D topographic effect is still present.

Consider the case $\rho_1 > \rho_2$. Here, at a short distance from the measuring line of the inhomogeneity edges and the ground surface topography in the Y-direction ($dy_{ter} = 1.2$ m (from -0.6 to 0.6) and $dy_{het} = 0.6$ m (from -3 to 3)), the 3D topographic effect prevails. Artifacts change with the change in the size of the topography and inhomogeneity in the YZ plane. When the edges of the inhomogeneity and topography are located at a distance of up to 2.8 m from the measuring line in the Y-direction, the effect of the shape of the inhomogeneity under the topography is also manifested more clearly.

At resistivity contrast ratio n equal to 0.5, 0.25, 0.17, 0.125, 0.1, 8, and 10, changes in apparent resistivity anomalies become more pronounced.

The greater the difference in resistivity between the inhomogeneity and the medium with the ground surface topography, the greater is the range of influence of the 3D effect.

4.1.3. The Influence of the Inhomogeneity's Size of the Medium under the Flat Ground Surface and under the Topography in the Y-Direction. To understand the influence

of the 3D effect of the inhomogeneity's size under smooth ground surface in the Y-direction on the 2D inversion, we set various dimensions of inhomogeneity dy_{het} = 0.6 m, 1.2 m, 2 m, 4 m, and 5.6 m. Respectively, the distance of the edge of the inhomogeneity from the measuring line was 0.3, 0.6, 1 2, and 2.8 m.

Calculations were made for the cases $\rho_1 < \rho_2$ and $\rho_1 > \rho_2$. We have set ρ_1 as $10 \, \Omega \cdot m$ and ρ_2 as $40 \, \Omega \cdot m$ when $\rho_1 < \rho_2$. We have set ρ_1 as $40 \, \Omega \cdot m$ and ρ_2 as $10 \, \Omega \cdot m$ when $\rho_1 > \rho_2$. The influence of the inhomogeneity's size of a 3D medium with a flat ground surface in the Y-direction on the results of 2D inversion is shown in Figure 8.

When the edges of the inhomogeneity were at distances of 0.3, 0.6, and 1 m (dy_{het} = 0.6, 1.2, and 2 m) from the measurements' line, in the geological section of the 2D inversion, obvious artifacts of the 3D effect can be noticed. The closer the edge of the inhomogeneity is to the survey line, the stronger the artifacts. Starting from a distance of 2 m (dy_{het} = 4 m) from the survey line, the 3D effect becomes insignificant.

To assess the influence of the size of 3D inhomogeneity under the ground surface with topography on the results of 2D inversion, we have set the same different sizes of inhomogeneity dy_{het} = 0.6, 1.2, 2, 4, and 5.6 m (corresponding distances of the edge of the inhomogeneity from the measuring line of the survey were 0.3, 0.6, 1, 2, and 2.8 m). The tests were made for media models with a slope angle of topography $\alpha = 30°$ and two topography widths equal to 1.2 m (from -0.6 to 0.6) and 5.6 m (from -2.8 to 2.8) on the y-axis. The influence of the inhomogeneity's size of a 3D medium with the ground surface topography in the Y-direction on the results of 2D inversion is shown in Figure 9.

Here, with a change in the size of the topography and inhomogeneity in the YZ plane, the artifacts become stronger. The closer the edges of the inhomogeneity and topography of the ground surface to the line of the survey, the stronger are the artifacts. This once again indicates that 3D geology and topography in the Y-direction, perpendicular to the survey line, will affect the results of 2D inversion.

4.1.4. The Distance of the Inhomogeneity from the Measuring Line. To estimate the possible range of the 3D effect influence of geological inhomogeneity, in this study, five types of immersed inhomogeneity distances perpendicular to the survey line were set, equal to disy$_{het}$ = 0, 0.3, 1, 1.5, and 2 m. The inhomogeneity was small. The dimensions of the inhomogeneity along the x −, y −, and z-axes were dx_{het} = 0.6 m, dy_{het} = 0.3 m, and dz_{het} = 0.43 m, respectively. For comparison, testing was carried out for two types of medium models, when the medium had a flat ground surface and when the medium had topography with different lengths in the Y-direction (dy_{ter} = 1.2, 2, 4, and 5.6 m). Calculations were made for the case $\rho_1 < \rho_2$ ($\rho_1 = 10 \, \Omega \cdot m$ and $\rho_2 = 40 \, \Omega \cdot m$) and $\rho_1 > \rho_2$ ($\rho_1 = 40 \, \Omega \cdot m$ and $\rho_2 = 10 \, \Omega \cdot m$). Figure 10 shows the influence of the inhomogeneity distance in the Y-direction on the results of 2D inversion for a 3D medium with a flat ground surface.

As shown in Figure 10, at distances disy$_{het}$ = 0 and 0.3 m, a 3D effect of geological inhomogeneity is significant.
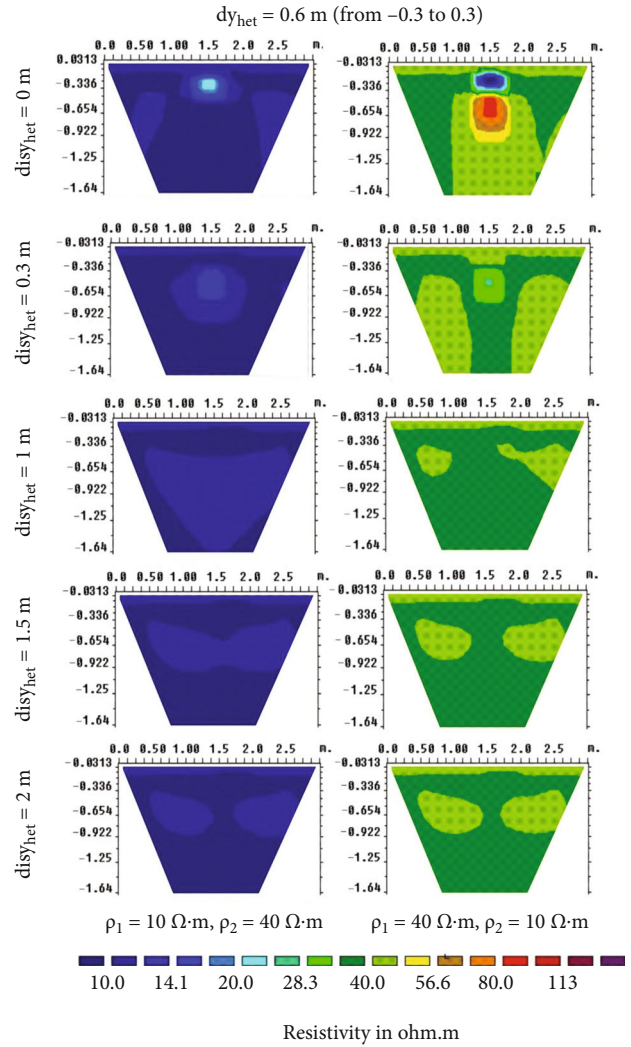

FIGURE 10: The influence of the inhomogeneity distance in the Y-direction on the results of 2D inversion for a 3D medium with a flat ground surface.

At distances disy$_{het}$ = 1, 1.5, and 2 m, the 3D effect gradually disappears.

Figure 11 shows the influence of the inhomogeneity distance in the Y-direction on the results of 2D inversion for a 3D medium with ground surface topography, corresponding to the case $\rho_1 < \rho_2$.

As shown in Figure 11, at distances disy$_{het}$ = 0 and 0.3 m, the results show an enhanced and mixed 3D effect caused by geological inhomogeneity and the uneven surface of the ground. Starting from the distance between the inhomogeneity and the measuring line disy$_{het}$ = 1 m and the size of the ground surface topography dy_{ter} = 2 m in the Y-direction, the 3D effect weakens.

4.1.5. Distance between Measuring Electrodes. To understand the influence of the distance between the measuring electrodes on the results of 2D ERT inversion at 3D topographic effects, different dx_{el} (0.125 m and 0.0625 m) and Num$_{el}$ (24 and 48) parameters were set for the same length of the
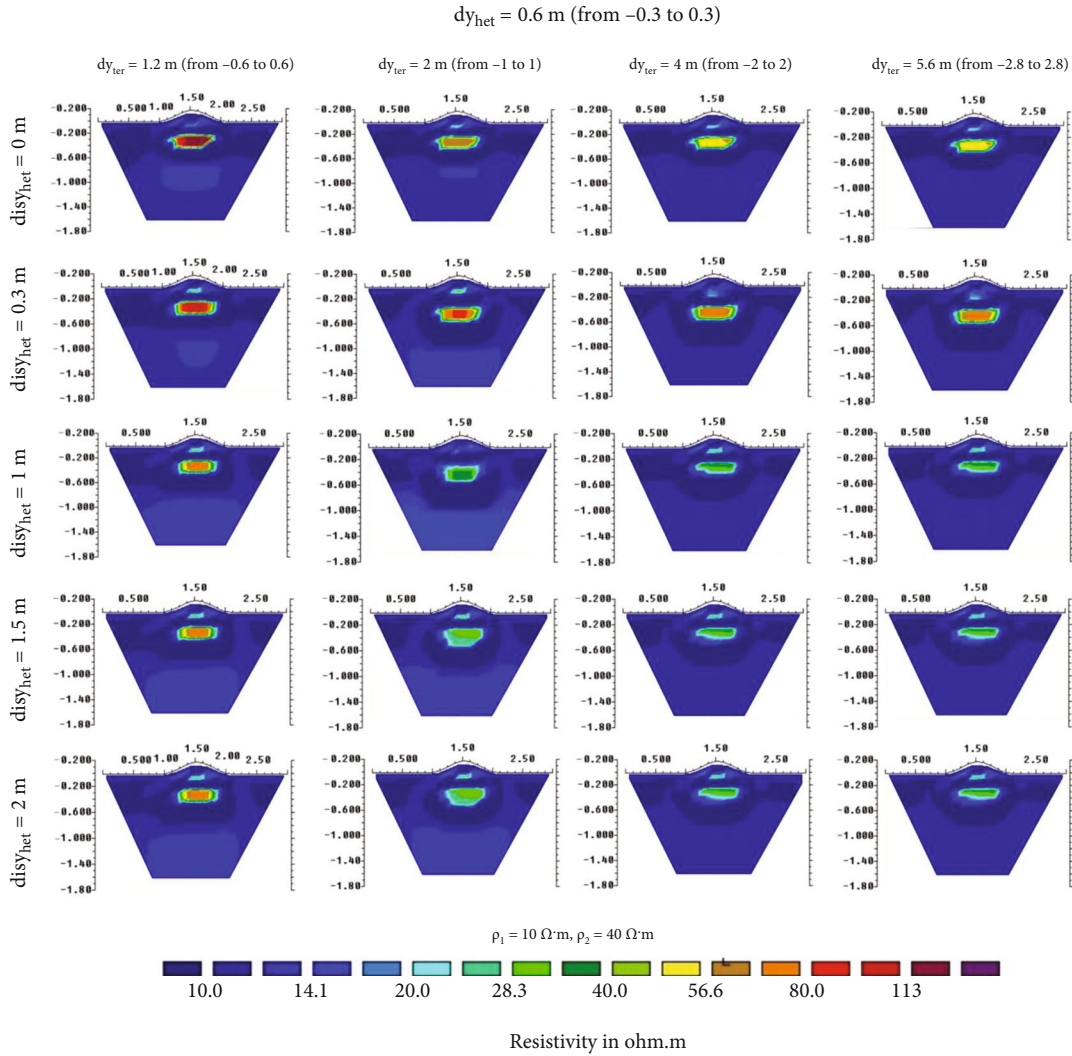
FIGURE 11: The influence of the inhomogeneity distance in the Y-direction on the results of 2D inversion for a 3D medium with ground surface topography ($\rho_1 < \rho_2$).

survey line equal to 3 m. The distance between the electrodes was reduced by half: $dx_{el} = 0.0625$ m. A model of a homogeneous 3D medium with ground surface topography was considered. The topography slope angle was $\alpha = 30°$ and the topography size is $dy_{ter} = 1.2$ m (from -0.6 to 0.6) along the y-axis. Figure 12 shows the influence of dx_{el} magnitude on the 3D topographic effect.

As the result shows, the reduction of the distance between the measuring electrodes did not significantly affect the 3D effect of the ground surface topography. The size of the anomaly caused by the 3D topographic effect has become slightly larger.

4.2. Discussion. 3D topographic effects caused by the ground surface topography lead to significant artifacts in geoelectric sections after performing a 2D inversion [39, 44]. Test 2D models cannot always show possible errors and artifacts when interpreting the results of 2D inversion, whereas the geoelectric section and topography are 3D [30, 40, 41]. Bievre et al. studied the influence of 3D topographic effects

on the 2D section inversion measured along the crest of the dam or on its average slope. The study was carried out using static and temporary ERT surveys during repair work on a small canal dam filled with earth in the center of France. They noted that 3D topographic effects affect the 2D inversion results. Displacements and some damage zones inside the dam may be related to the 3D distribution of resistivity underground, which cannot be taken into account using a 2D approach. Tresoldi et al. conducted tests on a small-scale prototype of a dam on a canal in San Giacomo delle Segnate, Mantua, northern Italy, to evaluate 3D effects and the effect of buried electrodes on the 2D ERT data processing results. The prototype of the dam represents a real site in the university laboratory with different water levels in the channel and different precipitations. They used a direct modeling approach (FEM) to evaluate 3D effects and the effect of buried electrodes in Res3Dmod software. Both the results of our study and Tresoldi et al. proved that an abnormal increase in resistivity values occurs due to the limitations of 2D surveys and models under the assumption that

$dy_{ter} = 1.2$ m (from −0.6 to 0.6)

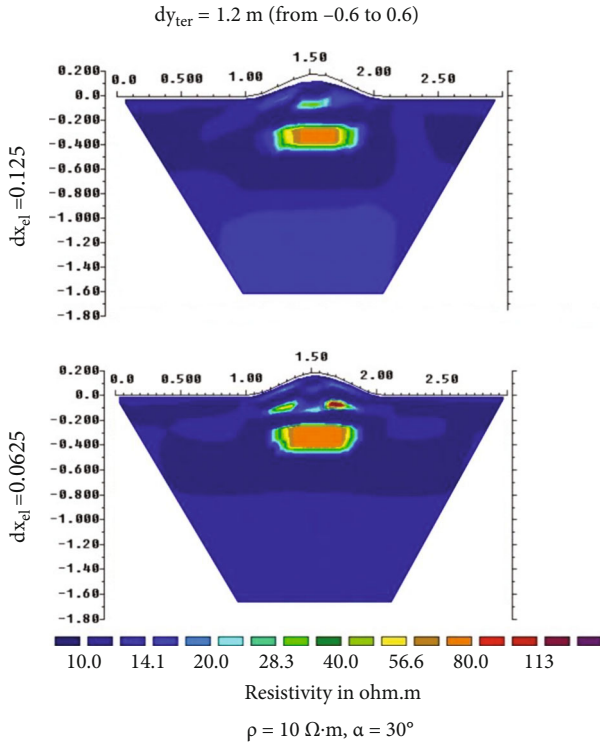$\rho = 10\ \Omega\cdot m,\ \alpha = 30°$

FIGURE 12: The influence of the distance between the measuring electrodes on 3D topographic effect.

the resistivity does not change in a perpendicular direction to the ERT profiles. For verification, they used 2D analytical calculations for a two-layer model of the ground and direct modeling performed in the Res2dmod software. Yilmaz and Coskun noticed that the results of 2D ERT inversion performed in areas with significant elevation changes may be erroneous, since the observed data on apparent resistivity may be distorted by topography.

The results of the study by Yang et al. have shown that 2D and 3D resistivity studies in the same place give very different images. The results of 2D ERT data inversion are greatly distorted by the influence of the 3D effect. Yin-Chun Hung et al. studied the influence of 3D effect and boundary effect on 2D ERT. They used a direct numerical simulation approach using FEM. They also studied the parametric change in the resistivity ratio, the distance between the electrodes, the depth of the pipeline insertion, and the average size to assess the influence of the 3D effect and the boundary effect on 2D ERT. However, their work considered a model of a 3D medium with a flat surface. In our work, to assess the 3D effect on the results of 2D inversion, we studied such factors of the 3D model influence as slope angle of the topography, the resistivity ratio of the inhomogeneity and the host medium, the average size of inhomogeneity and topography, the distance from the inhomogeneity to the measuring line for the medium with and without topography, and the distance between the electrodes of the ERT array. Thus, many studies devoted to 3D effects and 3D topographic effects consist in detecting and confirming the presence and influence of the 3D effect in the results of 2D ERT and 2D inversion. The results pre-

sented here also testify and confirm the influence of the 3D effect and the 3D topographic effect. In contrast from Tresoldi et al. and Yin-Chun Hung et al., in this study, calculations were performed using direct modeling by IEM, which is advantageous in saving computational resources and time.

Regarding the fact that the distortions of the vertical electrical sounding (VES) curves are not very noticeable in ridges and valleys with slope angles less than 20°, as Chanturishvili reported, can be seen in our study. However, it is confirmed here that it also depends on the size of the topography width dy_{ter} relative to the length of the survey line (perpendicular to the y-axis). Figure 13 shows graphs of apparent resistivity curves for different topography slope angles $(\alpha = 10°, 20°, 25°, \text{and } 30°)$ along the x-axis at the topography width $dy_{ter} = 1.2$ m. The edge of the hill is 0.6 m away from the survey line and is only about 1/5 of the length of the survey line. In this case, there are more pronounced artifacts in the 2D inversion results and this can also be seen on the graph of the apparent resistivity curves typical for a convex shape of the topography [27]. With an increase in the topography slope angle $(\alpha = 30°)$, the changes in the apparent resistivity curve also increase.

Figure 14 shows graphs of apparent resistivity curves to assess the influence of the resistivity contrast ratio of the inhomogeneous medium with the 3D ground surface topography in the results of 2D ERT data inversion. The corresponding graphs of the apparent resistivity curves show the relationship between changes in the resistivity contrast ratio when $\rho_1 < \rho_2$ ($n = 2, 4, 6, 8, \text{and } 10$) and $\rho_1 > \rho_2$ ($n = 0.5, 0.25, 0.17, 0.125, \text{and } 0.1$).

In the case of $\rho_1 < \rho_2$ (Figures 14(a) and 14(b)), it can be seen from the graphs of the apparent resistivity curves that the 3D topographic effect has a stronger influence, as mentioned above. In almost all cases, the behavior of curves inherent for the convex shape of the topography prevails.

In the case $\rho_1 > \rho_2$ (Figures 14(c) and 14(d)), it can be seen from the graphs of the apparent resistivity curves that the 3D topographic effect is present, but due to the low resistivity of the inhomogeneity, it is possible to notice the predominance of the curve nature inherent in the medium without topography and with inhomogeneity, the resistivity of which is $\rho_2 = 10\ \Omega\cdot m$. The graphs of the curves in this case also confirm the results of 2D inversion that the influence of the inhomogeneity shape under the topography becomes clearer.

Figure 15 shows graphs of the apparent resistivity curves of a medium with topography and heterogeneity for the case with $dy_{ter} = 1.2$ m, $dy_{het} = 0.6$ m and $dy_{ter} = 5.6$ m, and $dy_{het} = 5.6$ m ($n = 10$), which show a greater deviation of the apparent resistivity curves at the topography width $dy_{ter} = 1.2$ m. This indicates the predominance of 3D topographic effect, which leads to serious artifacts in the results of 2D inversion.

The graphs of the curves are compared in Figures 16 and 17.

In Figure 16, we can see a comparison of curves, which also indicates the influence of the 3D topographic effect. According to the graph for an inhomogeneous medium with topography, it is noticeable how the behavior of the apparent
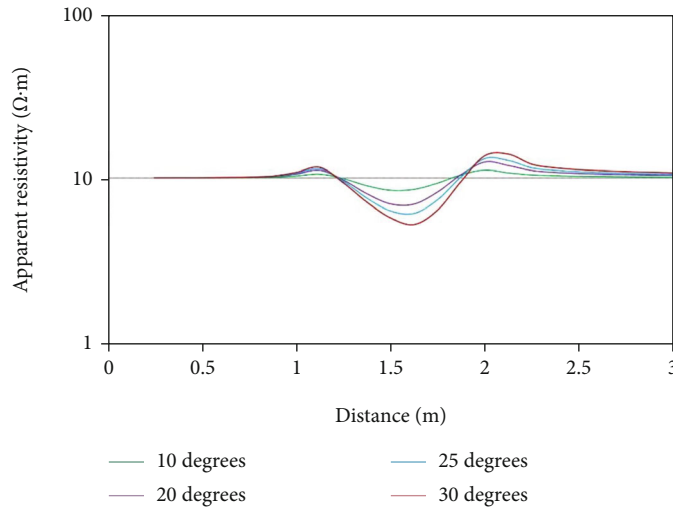
FIGURE 13: Graphs of apparent resistivity curves for different topography slope angle (at the topography width $dy_{ter} = 1.2$ m).
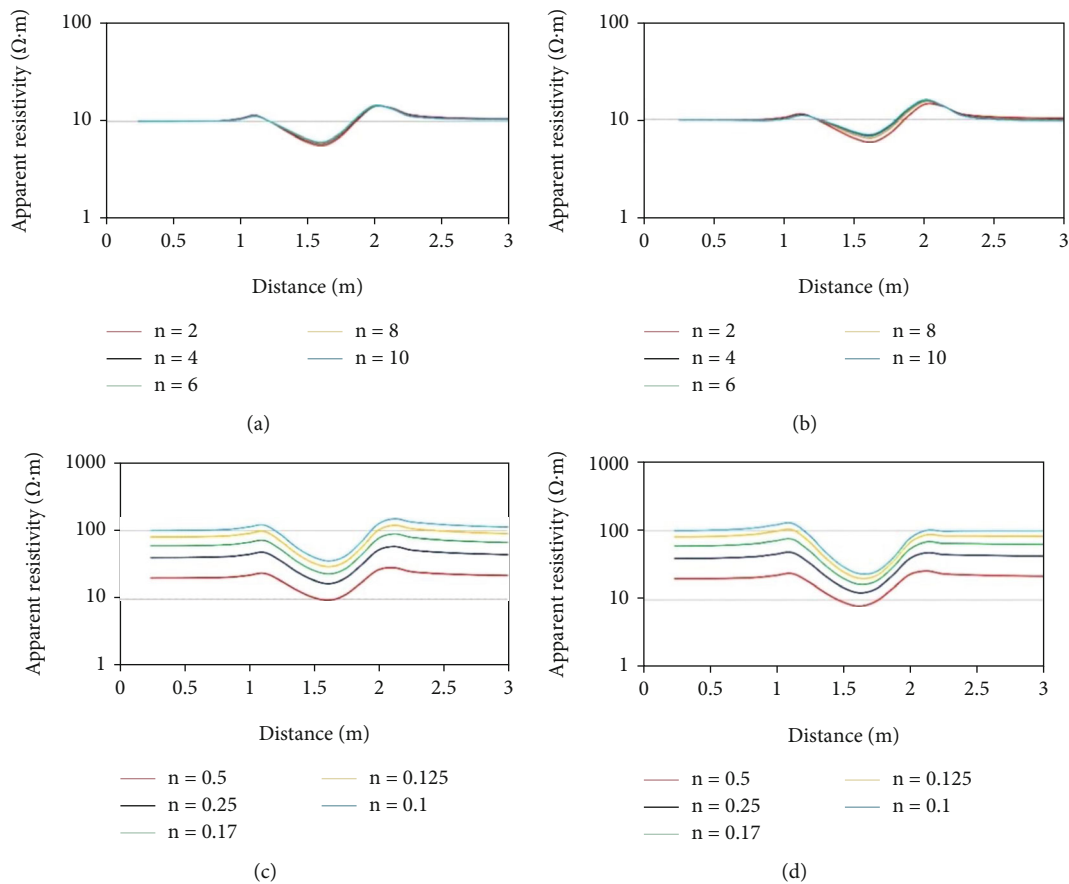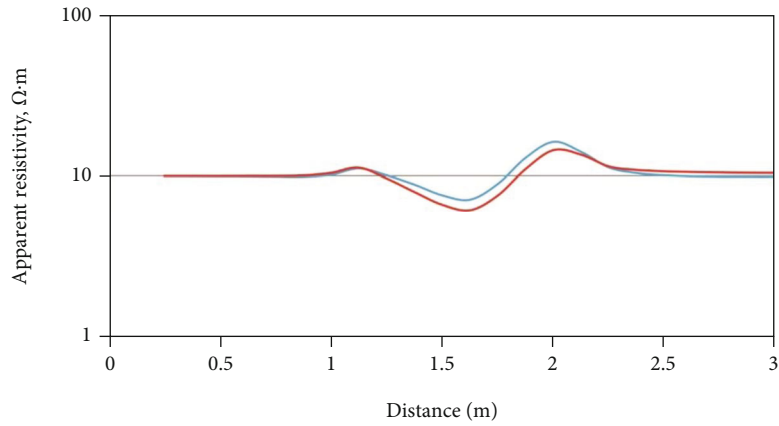

(a)

(b)

(c)

(d)

FIGURE 14: Graphs of apparent resistivity curves for the cases when (a) $\rho_1 < \rho_2$ and $dy_{ter} = 1.2$ m, $dy_{het} = 0.6$ m; (b) $\rho_1 < \rho_2$ and $dy_{ter} = 5.6$ m, $dy_{het} = 5.6$ m; (c) $\rho_1 > \rho_2$ and $dy_{ter} = 1.2$ m, $dy_{het} = 0.6$ m; and (d) $\rho_1 > \rho_2$ and $dy_{ter} = 1.2$ m, $dy_{het} = 0.6$ m.

resistivity curve is similar to the behavior of the curve for a homogeneous medium with topography. This explains the difficulty of detecting inhomogeneity under the topography in this case.

In Figure 17, one can also note the influence of the 3D topographic effect, and here, the nature of the curve of the
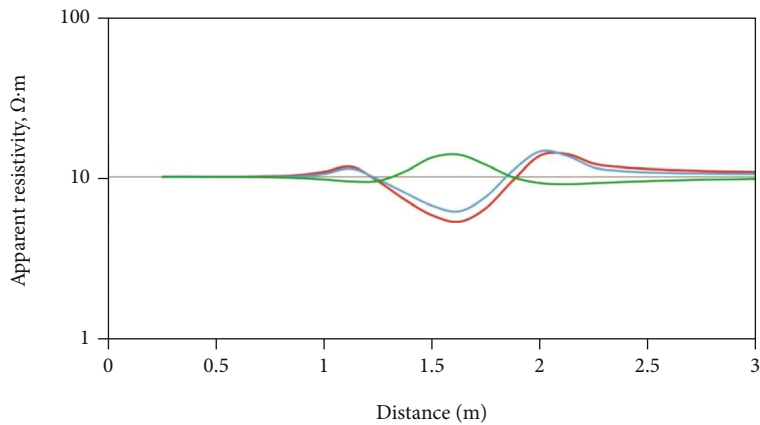
medium with topography and heterogeneity is closer to the nature of the curve of the medium with topography and without heterogeneity.

Thus, we investigated the influence of 3D topographic effect of homogeneous and inhomogeneous media on the results of 2D ERT data inversion. The corresponding results

For the medium with
topography and heterogeneity
$\rho_1 = 10\ \Omega\cdot m$, $\rho_2 = 100\ \Omega\cdot m$

— $dy_{ter} = 5.6$ m (from −2.8 to 2.8)
$dy_{het} = 5.6$ m (from −2.8 to 2.8)

— $dy_{ter} = 1.2$ m (from −0.6 to 0.6)
$dy_{het} = 0.6$ m (from −0.3 to 0.3)

FIGURE 15: Graphs of apparent resistivity curves for the medium with topography and inhomogeneity for the cases $dy_{ter} = 1.2$ m, $dy_{het} = 0.6$ m and $dy_{ter} = 5.6$ m, and $dy_{het} = 5.6$ m ($n = 10$).

$\rho_1 = 10\ \Omega\cdot m$, $\rho_2 = 100\ \Omega\cdot m$

For the medium with
— topography and without heterogeneity
$dy_{ter} = 1.2$ m (from −0.6 to 0.6)

For the medium with
topography and heterogeneity
— $dy_{ter} = 1.2$ m (from −0.6 to 0.6)
$dy_{het} = 0.6$ m (from −0.3 to 0.3)

For the medium with
— heterogeneity and without topography
$dy_{het} = 0.6$ m (from −0.3 to 0.3)

FIGURE 16: Comparative graph of apparent resistivity curves ($\rho_1 < \rho_2$, $n = 10$).

$\rho_1 = 100\ \Omega \cdot m,\ \rho_2 = 10\ \Omega \cdot m$

— For the medium with heterogeneity and without topography $dy_{het} = 0.6$ m (from -0.3 to 0.3)

— For the medium with topography and without heterogeneity $dy_{ter} = 1.2$ m (from -0.6 to 0.6)

— For the medium with topography and heterogeneity $dy_{ter} = 1.2$ m (from -0.6 to 0.6) $dy_{het} = 0.6$ m (from -0.3 to 0.3)
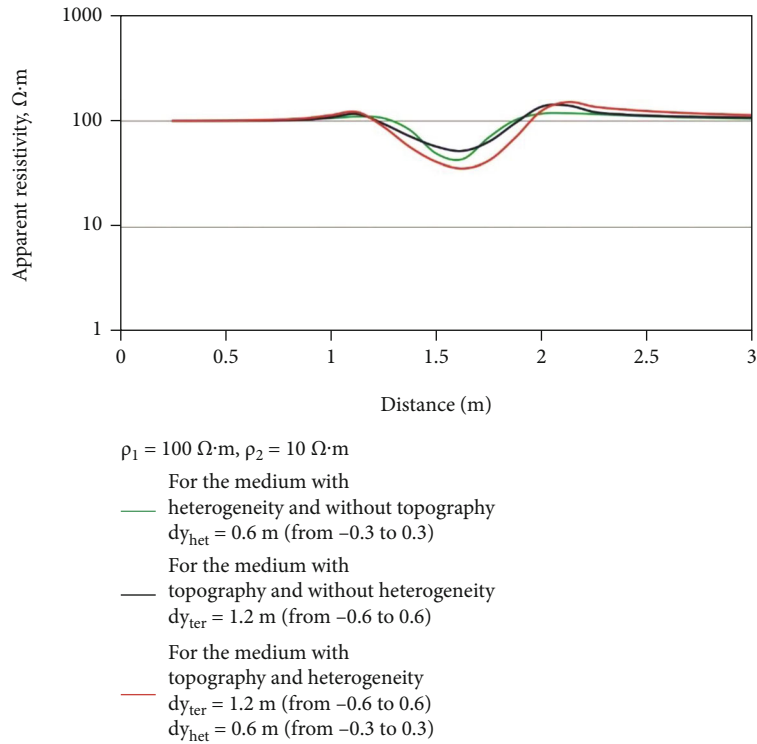
FIGURE 17: Comparative graph of apparent resistivity curves ($\rho_1 > \rho_2$, $n = 0.1$).

can be used in the future as a guide in the processing and interpretation of 2D ERT data.

5. Conclusions

The conducted research leads to the following conclusions and recommendations when testing and interpreting 2D inversion profiles of ERT:

(1) As the width of the hill increases in the Y-direction compared to the length of the survey line, the amplitude of the inversion artifacts decreases. The size of the artifacts is inversely proportional to the width of the hill in the Y-direction. Due to the truncation of the hill in the Y-direction, the 3D topographic effect increases

(2) Artifacts increase with an increase in the topography slope angle along the x - and y -axes at the same width of the hill, because, with an increase in the slope of the hill, the height of the hill also increases. In our case, with an increase in the height and the slope angle of the hill along the x-axis, the slope angle along the y-axis increases, respectively

(3) The greater the contrast in resistivity between the inhomogeneity and the medium with the ground surface topography, the greater is the range of influence of the 3D effect. The 3D topographic effect prevails in sections of 2D inversion

(4) The closer the edges of the inhomogeneity and topography of the ground surface are to the measuring line

of the survey (perpendicularly), the stronger the artifacts caused by the 3D effect. 3D geology and topography in the Y-direction, perpendicular to the survey line, definitely affect the results of 2D inversion

(5) The 3D effect caused by inhomogeneity influences at a distance up to a third of the length of the measuring line (Len$_{sur}$ = 3 m). The 3D effects, caused by inhomogeneity and the 3D topographic effect, are mixed and amplified

(6) Different distances between measuring electrodes have shown that it is impractical to use the distance between the electrodes as a parameter, normalizing 3D topographic effects

Displaying artifacts caused by different hill widths in the Y-direction compared to the length of the survey line can be useful when interpreting ERT data, since this allows to assess by a topographic map whether changes will significantly affect results.

Data Availability

The data used to support the findings of this study are included within the article.

Conflicts of Interest

The authors declare that there are no conflicts of interest regarding the publication of this paper.

References

[1] D. A. Kvon, I. N. Modin, V. A. Shevnin, D. V. Makarov, and A. D. Skobelev, "Electrical resistivity tomography for identification of frozen and cooled saline ground," *Kriosfera Zemli*, vol. 23, no. 3, pp. 3–12, 2019.

[2] A. D. Skobelev, V. S. Serebryakov, E. Y. Matlakhova, A. P. Ermakov, I. N. Modin, and M. I. Bogdanov, "Geophysical studies of SUBSURFACE gas SEEPAGE in SAND-CLAY soils," *Engineering Surveys*, vol. 12, no. 3-4, pp. 70–80, 2018.

[3] K. Kielbasinski, P. Dobak, L. Kaczmarek, and S. Kowalczyk, "The influences of local glacitectonic disturbance on overconsolidated clays for upland slope stability conditions: a case study," *Applied Sciences*, vol. 11, no. 22, p. 10718, 2021.

[4] M. Mele, D. Servida, and D. Lupis, "Characterisation of sulphide-bearing waste-rock dumps using electrical resistivity imaging: the case study of the Rio Marina mining district (Elba Island, Italy)," *Springer Science + Business Media Dordrecht 2012*, vol. 185, no. 7, pp. 5891–5907, 2013.

[5] A. V. Minaev, V. V. Minaev, and A. N. Suturin, "Detection by electrical resistivity tomography of subaqual discharge zones of groundwater (water area of the village Listvyanka)," *Earth Science*, vol. 66, no. 12, pp. 176–180, 2017.

[6] P. Yogeshwar, S. Hamacher, H. Reçi, T. Hauck, K. Onuzi, and B. Tezkan, "Investigating sedimentological architecture using electrical resistivity tomography: a case study from the archaeological open-air site Shën Mitri, Southern Albania," *Pure and Applied Geophysics*, vol. 176, no. 2, pp. 843–856, 2019.

[7] A. A. R. Zohdy, "A new method for the automatic interpretation of Schlumberger and Wenner sounding curves," *Geophysics*, vol. 54, no. 2, pp. 245–253, 1989.

[8] R. D. Barker, "A simple algorithm for electrical imaging of the subsurface," *First Break*, vol. 10, no. 2, pp. 53–62, 1992.

[9] M. Schoor, "Detection of sinkholes using 2D electrical resistivity imaging," *Journal of Applied Geophysics*, vol. 50, no. 4, pp. 393–399, 2002.

[10] D. Demanet, E. Pirard, F. Renardy, and D. Jongmans, "Application and processing of geophysical images for mapping faults," *Computational Geosciences*, vol. 27, no. 9, pp. 1031–1037, 2001.

[11] F. T. Nguyen, S. Garambois, D. Jongmans, E. Pirarda, and M. H. Loke, "Image processing of 2D resistivity data for imaging faults," *Journal of Applied Geophysics*, vol. 57, no. 4, pp. 260–277, 2005.

[12] M. H. Loke and R. D. Barker, "Practical techniques for 3D resistivity surveys and data inversion electrical imaging surveys," *Geophysical Prospecting*, vol. 44, no. 3, pp. 499–523, 1996.

[13] C. Rucker, T. Gunther, and K. Spitzer, "Three-dimensional modelling and inversion of dc resistivity data incorporating topography – I. modelling," *Geophysical Journal International*, vol. 166, no. 2, pp. 495–505, 2006.

[14] T. Gunther, C. Rucker, and K. Spitzer, "Three-dimensional modelling and inversion of dc resistivity data incorporating topography – II. Inversion," *Geophysical Journal International*, vol. 166, no. 2, pp. 506–517, 2006.

[15] T. Gunther and C. Rucker, *Boundless electrical resistivity tomography in BERT 2*, The User Tutorial, 2019, Version 2.2.8.

[16] A. Pidlisecky, E. Haber, and R. Knight, "RESINVM3D: a 3D resistivity inversion package," *Geophysics*, vol. 72, no. 2, pp. H1–H10, 2007.

[17] A. E. Kaminsky, S. A. Erokhin, and A. V. Politcina, "Total data inversion of shallow geophysical surveys," *Engineering Surveys*, vol. 9, pp. 44–51, 2016.

[18] M. Karaoulis, A. Revil, P. Tsourlos, D. D. Werkema, and B. J. Minsley, "IP4DI: a software for time-lapse 2D/3D DC-resistivity and induced polarization tomography," *Computers & Geosciences*, vol. 54, pp. 164–170, 2013.

[19] J. H. Coggon, "Electromagnetic and electrical modeling by the finite element method," *Geophysics*, vol. 36, no. 1, pp. 132–155, 1971.

[20] I. R. Mufti, "Finite-difference RESISTIVITY modeling for ARBITRARILY SHAPED TWO-DIMENSIONAL structures," *Geophysics*, vol. 41, no. 1, pp. 62–78, 1976.

[21] W. H. Pelton, L. Rijo, and C. M. Swift Jr., "Inversion of two dimensional resistivity and induced polarization data," *Geophysics*, vol. 43, no. 4, pp. 788–803, 1978.

[22] A. Dey and H. F. Morrison, "Resistivity modelling for arbitrarily shaped two-dimensional structures," *Geophysical Prospecting*, vol. 27, no. 1, pp. 106–136, 1979.

[23] M. H. Loke and R. D. Barker, "Least-squares deconvolution of apparent resistivity pseudosections," *Geophysics*, vol. 60, no. 6, pp. 1682–1690, 1995.

[24] M. H. Loke and R. D. Barker, "Rapid least-squares inversion of apparent resistivity pseudosections by a quasi-Newton method1," *Geophysical Prospecting*, vol. 44, no. 1, pp. 131–152, 1996.

[25] A. V. Veshev, "Influence of relief on the combined profiling results," *Scientific Notes of LSU*, vol. 278, no. 11, 1959.

[26] V. M. Zaporozhets, "The influence of relief on the results of resistance measurements (based on the works of S.G. Komarov and L. P. Gorbenko)," in *Elkageer*, vol. 4, no. 12, 1938.

[27] L. C. Chanturishvili, "Investigation of the distortion of a uniform electric field in the medium, depending on the roughness of the earth-air interface," *Special cases. Dissertation submitted for the Candidate of Physical and Mathematical Sciences degree*, Tbilisi, 1947.

[28] R. C. Fox, G. W. Hohmann, and L. Rijo, *Topographic effects in resistivity surveys*, Earth Science Laboratory University of Utah Research Institute, 1978.

[29] R. C. Fox, G. W. Hohmann, T. J. Killpack, and L. Rijo, "Topographic effects in resistivity and induced-polarization surveys," *Geophysics*, vol. 45, no. 1, pp. 75–93, 1980.

[30] S. Yilmaz and N. Coskun, "A study of the terrain-correction technique for the inhomogeneous case of resistivity surveys," *Scientific Research and Essays*, vol. 6, no. 24, pp. 5213–5223, 2011.

[31] P. Queralt, J. Pous, and A. Marcuello, "2-D resistivity modeling: an approach to arrays parallel to the strike direction," *Geophysics*, vol. 56, no. 7, pp. 941–950, 1991.

[32] M. H. Loke, "Topographic modelling in resistivity imaging inversion," in *Proceedings of the 62nd EAGE Conference and Technical Exhibition, Extended Abstracts*, pp. 1–4, Glasgow, Scotland, 2000.

[33] E. Erdogan, I. Demirci, and M. E. Candansayar, "Incorporating topography into 2D resistivity modeling using finite-element and finite-difference approaches," *Geophysics*, vol. 73, no. 3, pp. F135–F142, 2008.

[34] I. Demirci, E. Erdogan, and M. E. Candansayar, "Two-dimensional inversion of direct current resistivity data incorporating topography by using finite difference techniques with triangle

cells: investigation of Kera fault zone in western Crete," *Geophysics*, vol. 77, no. 1, pp. E67–E75, 2012.

[35] S. Penz, H. Chauris, D. Donno, and C. Mehl, "Resistivity modelling with topography," *Geophysical Journal International*, vol. 194, no. 3, pp. 1486–1497, 2013.

[36] H. T. Holcombe and G. R. Jiracek, "Three-dimensional terrain corrections in resistivity surveys," *Geophysics*, vol. 49, no. 4, pp. 439–452, 1984.

[37] L. Tong and C. Yang, "Incorporation of topography into two dimensional resistivity inversion," *Geophysics*, vol. 55, no. 3, pp. 354–361, 1990.

[38] P. Tsourlos, J. E. Szymanski, and G. Tsokas, "The effect of terrain topography on commonly used resistivity arrays," *Geophysics*, vol. 64, no. 5, pp. 1357–1363, 1999.

[39] G. Tresoldi, A. Hojat, and L. Zanzi, *Correcting the influence of 3d geometry to process 2d ERT monitoring data of river embankments at the laboratory scale*, GNGTS, 2018.

[40] H. Yin-Chun, L. Chih-Ping, L. Chin-Tan, and W. Ko-Wei, "3D and boundary effects on 2D electrical resistivity tomography," *Applied Sciences*, vol. 9, no. 15, p. 2963, 2019.

[41] X. Yang and M. Lagmanson, "Comparison of 2D and 3D electrical resistivity imaging methods," in *Symposium on the Application of Geophysics to Engineering and Environmental Problems*, pp. 585–594, 2006.

[42] T. Dahlin, "2D resistivity surveying for environmental and engineering applications," *First Break*, vol. 14, no. 7, pp. 275–283, 1996.

[43] C. P. Lin, Y. C. Hung, P. L. Wu, and Z. H. Yu, "Performance of 2-D ERT in investigation of abnormal seepage: a case study at the Hsin-Shan earth dam in Taiwan," *Journal of Environmental and Engineering Geophysics*, vol. 19, no. 2, pp. 101–112, 2014.

[44] G. Bievre, L. Oxarango, T. Günther, D. Goutaland, and M. Massardi, "Improvement of 2D ERT measurements conducted along a small earth-filled dyke using 3D topographic data and 3D computation of geometric factors," *Journal of Applied Geophysics*, vol. 153, pp. 100–112, 2018.

[45] A. Hojat, D. Arosio, M. H. Loke et al., "Assessment of 3D geometry effects on 2D ERT data of a permanent monitoring system along a river embankment," *EAGE-GSM 2nd Asia Pacific Meeting on Near Surface Geoscience and Engineering*, vol. 2019, pp. 1–5, 2019.

[46] B. Mukanova and I. Modin, *The boundary element method in geophysical survey*, Springer, 2018.

[47] B. Mukanova, T. Mirgalikyzy, and D. Rakisheva, "Modelling the influence of ground surface relief on electric sounding curves using the integral equations method," *Mathematical Problems in Engineering*, vol. 2017, Article ID 9079475, 10 pages, 2017.

[48] T. Mirgalikyzy, B. Mukanova, and I. Modin, "Method of integral equations for the problem of electrical tomography in a medium with ground surface relief," *Journal of Applied Mathematics*, vol. 2015, Article ID 207021, 10 pages, 2015.

[49] B. Mukanova and T. Mirgalikyzy, "Modeling the impact of relief boundaries in solving the direct problem of direct current electrical sounding," *Communications in Computer and Information Science*, vol. 549, pp. 117–123, 2015.

[50] K. I. Baranchuk, T. M. Mirgalikyzy, I. N. Modin, and B. G. Mukanova, "Physical modeling of electrical resistivity tomography on ground surface with a complex relief," *Engineering Survey*, vol. 1, no. 11, pp. 56–65, 2017.

[51] T. Mirgalikyzy, "Influence of the ground surface relief on the results of electrical tomography," in *24th European Meeting of Environmental and Engineering Geophysics, Conference Proceedings*, vol. 2018, Porto, Portugal, September 2018.

[52] V. I. Dmitriev and I. S. Barashkov, "Finite-difference–integral method for computing low-frequency electromagnetic fields in a nonhomogeneous medium," *Computational Mathematics and Modeling*, vol. 27, no. 2, pp. 145–161, 2016.

[53] B. Mukanova, T. Mirgalikyzy, and M. Turarova, "Numerical aspects of the adaptive computational grid in solving the problems of electrical prospecting with direct current," *International Journal of Mathematics and Physics*, vol. 9, no. 2, pp. 4–12, 2018.

[54] M. Turarova, T. Mirgalikyzy, B. Mukanova, and P. Kaznacheev, "Simulation of electrical resistivity tomography curves in a three-dimensional medium with a ground surface relief and immersed inhomogeneity," in *International Conference on Information Science and Communications Technologies (ICISCT)*, Tashkent, Uzbekistan, November 2019.

[55] M. K. Turarova, P. A. Kaznacheev, B. G. Mukanova, I. N. Modin, and T. Mirgalikyzy, "The algorithm for calculating the electric field by the integral equations method in a conductive medium with 3D local inhomogeneity and uneven relief of the ground surface," *Bulletin of the Kazakh-British Technical University (KBTU)*, vol. 17, no. 53, pp. 205–217, 2020.